THE JOURNAL OF PHYSICAL CHEMISTRY B

Article

pubs.acs.org/JPCB

Charge-Induced Patchy Attractions between Proteins

Weimin Li,[†] Björn A. Persson,[‡] Maxim Morin,[†] Manja A. Behrens,[†] Mikael Lund,*[,‡] and Malin Zackrisson Oskolkova*[,†]

[†]Division of Physical Chemistry and [‡]Division of Theoretical Chemistry, Lund University, POB 124, 22100 Lund, Sweden

ABSTRACT: Static light scattering (SLS) combined with structure-based Monte Carlo (MC) simulations provide new insights into mechanisms behind anisotropic, attractive protein interactions. A nonmonotonic behavior of the osmotic second virial coefficient as a function of ionic strength is here shown to originate from a few charged amino acids forming an electrostatic attractive patch, highly directional and complementary. Together with Coulombic repulsion, this attractive patch results in two counteracting electrostatic contributions to the interaction free energy which, by operating over different length scales, is manifested in a subtle, salt-induced minimum in the second virial coefficient as observed in both experiment and simulations.

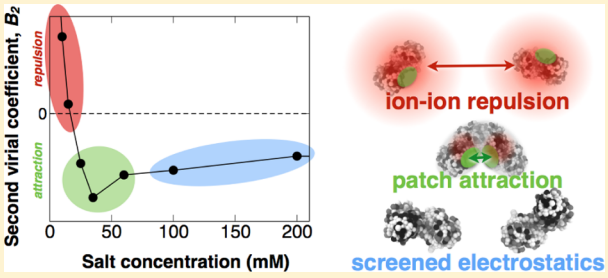

INTRODUCTION

Understanding how protein−protein interactions originate from the level of specific amino acids is of great importance to discern protein function and solution behavior.[1] Due to the inherent complexity, this is a considerable challenge[2−4] because both protein shape and interactions are anisotropic where surface-localized amino acid residues create irregular patterns of neutral, charged, and hydrophobic regions. Overall, these regions or patches contribute to the anisotropic protein interaction energy in a complex manner that ultimately governs if the protein undergoes crystallization, phase separation, and aggregation.[2,3,5,6]

A recent study shows that protein crystallization is often dominated by a limited number of amino acid contacts,[7] giving rise to patchy protein−protein interactions.[5] Describing proteins as patchy, spherical colloids is expected to change the overall phase diagram as compared to that of particles interacting via a centrosymmetric potential.[8−12] It is, however, nontrivial to map the effect of specific amino acid sequences onto such models and more granular approaches seem warranted to study the effect of, i.e., point mutations, solution pH, and salt concentration.

Dissecting which noncovalent, intermolecular interactions that dominate under certain solution conditions is difficult. Experiments probing, i.e., the osmotic second virial coefficient, B_2, does not allow for a separation of the different contributions to the overall interaction. The virial coefficient nontheless remains an important, experimentally accessible quantity that provides a thermodynamic measure of protein−protein interactions.

In this work, we combine static light scattering measurements of B_2 with Metropolis Monte Carlo (MC) simulations from which B_2 is calculated by taking into account the detailed protein structure as well as solution conditions. We show how protein interactions operate in a delicate balance of several both attractive and repulsive contributions, resulting in an electrostatic patchy attraction. The mechanism is recognized both in SLS experiments and in the MC simulations via a nonmonotonous ionic strength dependence of the second virial coefficient at low to moderate ionic strengths, where salt first lowers B_2 and then increases it. To determine which mechanism is responsible for the observed nonmonotonic behavior, we consider also the possibility of Kirkwood fluctuation forces, which are attractive protein−protein interactions due to correlated protonation states in the two proteins.[13,14] This was, however, dismissed by allowing the amino acids to titrate, following a proton titration scheme implemented in the simulations.[14] Left to consider are two electrostatic contributions counteracting each other. The first is a generic, screened Coloumb repulsion due to the net charge of the protein at the studied conditions; the second is a local patch in the charge distribution resulting in a directional, attractive patch.[15] Further, the simulations show that electrostatic interactions alone are insufficient and that there is a nonadditive coupling with van der Waals interactions. Similar salt-screened attractions appearing at low-to-intermediate ionic strengths have previously been observed in several experimental studies of proteins.[6,16,17] Also, more recently, a nonmonotonic behavior of B_2 for monoclonal antibodies was found[18] and the authors indeed argued for a similar mechanism. This body of data points to the possibility of electrostatic attractive patchiness, with a high complementarity, which if present, would appear at low ionic strength and in the neighborhood of the isoelectric point.

METHODS

Sample Preparation. We use bovine lactoferrin[19,20] (>96% purity, Morinaga Milk Industry Co., Ltd., Japan), a globular

Received: December 2, 2014
Revised: December 10, 2014
Published: December 10, 2014

DOI: 10.1021/jp512027j
J. Phys. Chem. B 2015, 119, 503−508

milk protein with a molecular weight of 80 kDa.[21] Lactoferrin resembles the shape of a dumbbell, as can be seen in Figure 1,

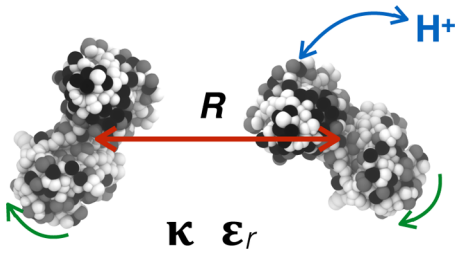

Figure 1. Monte Carlo model of two lactoferrin molecules built from collections of amino acid beads that can be neutral (white spheres), cationic (black spheres), or anionic (gray spheres). Solvent and salt particles are treated implicitly by the relative dielectric constant, ϵ_r, and the inverse Debye screening length, κ. During thermal averaging, the proteins translate (red), rotate (green), and fluctuate (blue) according to solution pH and intermolecular interactions.[14]

with the half-axis equal to 4.7 and 2.6 nm.[22] The isoelectric point (pI) is estimated to be 9.4 from titration simulations,[15] slightly higher than the experimental value of 9.[23] In this study we perform our experiments at pH $\leq$ 7. Stock solutions of lactoferrin were prepared at a concentration of 2 mg/mL by dissolving in NaOAc buffer, I = 5 mM, at pH 5.5 $\pm$ 0.02. We use the Henderson–Hasselbalch equation to account for the contribution to the ionic strength due to changes in dissociation of the buffer species with pH. Also, 1 mM NaN_3 was included to prevent microbial growth; this was also accounted for in the ionic strength.

The chemical nature of salt and buffer components were specifically chosen to be monovalent to avoid ion adsorption, which can dramatically change protein interactions.[24] A stock solution was equilibrated for at least 48 h at room temperature to allow for sufficient solubilization, after which an extensive filtration (centrifugal filters, Millipore) procedure was performed to remove possible contaminants and aggregates. Satisfactory buffer exchange was reached when the filtrate reached the desired target pH ($\pm$0.02). We stress the importance to remove contaminants and insoluble aggregates, which are present in the commercial powder, to obtain experimental B_2 values in close agreement with values from simulations. At low pH we used NaOAc buffer, and at higher pH, Tris buffer, both chosen to produce only monovalent buffer components. Overall, this procedure results in monomeric protein solutions that were monitored by dynamic light scattering (DLS) prior to and after each measurement. DLS allows for extraction of the hydrodynamic radius r_H of the solute species from the cumulant expansion of the autocorrelation function and by the CONTIN analysis[25,26] where a convolution of the distribution was consistent with the presence of a single protein species of same size. Throughout this study, samples contained a hydrodynamic radius of approximately 4 nm in good agreement with literature.[21] A constant temperature of 25 $\pm$ 0.1 °C was used throughout all experimental measurements. Determination of the protein concentration was done by UV absorption spectroscopy; the absorption coefficient was determined to be 1.224 $\pm$ 0.004 cm^2/mg using only monomeric samples, monitored by DLS, to avoid incorrect concentration determination due to contributions from light scattering of aggregates. The static and dynamic light scattering experiments were performed using an ALV 5000F CGS-8F goniometer (ALV, Germany) and correlator equipped with a He–Ne laser diode (Spectra Physics, 127 V/50 mW), operating at a wavelength λ = 632.8 nm.

Experimental Determination of Second Virial Coefficients. Static light scattering allows for determination of the molecular weight M_w and the second virial coefficient B_2 of solutions, which is the property of interest here. B_2 is an important property of the overall interactions where a positive value indicates overall repulsive protein interactions and a negative value signals overall attractive interactions. It is determined by using the relationship between the Rayleigh ratio, R_θ (m^{-1}), and the mass concentration of the protein C (kg/m^3), referred to as a Debye plot

$$\frac{KC}{R_\theta} = \frac{1}{M_w} + \frac{2N_A B_2}{M_w^2} C \tag{1}$$

where

$$K = \frac{4\pi^2 n_0^2 (dn/dC)^2}{N_A \lambda^4} \tag{2}$$

In eq 1 and eq 2 N_A is Avogadro's number, n_0 is the refractive index of the buffer solution, λ (m) is the wavelength, and dn/dC (m^3/kg) is the increment in the refractive index with respect to increasing protein concentration. In all measurements, static and dynamic light scattering experiments were performed in parallel, at a fixed angle of 90°. However, angular scans were performed initially to ensure no angular dependence. The refractive indices of the buffer solutions, n_0, were measured on an Abbe refractometer. For the refractive index increment, dn/dC, a standard literature value for globular proteins (0.000 186 m^3/kg)[27] was used, which returned molecular weights in close agreement with the literature value of 80 kDa.[21] The same molecular weight was used to determine the B_2 values from the slope in the Debye plots.

Monte Carlo Simulations. Metropolis Monte Carlo (MC) computer simulations[28] were used to compute the Helmholtz interaction free energy between two rigid lactoferrin molecules in an aqueous salt solution. Amino acids are represented by spheres located at the residue mass center according to the crystal structure (PDB 1BLF), Figure 1. The canonical (NVT) ensemble is sampled using molecular translational and rotational MC moves as well as proton swap moves on titratable (acid and basic) sites to account for charge fluctuations; i.e., the simulations are performed at constant pH.[14] Production runs consist of at least 10^8 configurations, preceded by 10 times shorter equilibration runs. Solvent and salt are treated at the Debye–Hückel level whereas exchange repulsion and short-ranged attractions, such as van der Waals (vdW), are described by a Lennard-Jones potential, yielding the effective system energy

$$\beta u = \sum_{i\neq j}^{N} \lambda_B z_i z_j \exp(-\kappa r_{ij})/r_{ij} + 4\beta\epsilon[(\sigma_{ij}/r_{ij})^{12} - (\sigma_{ij}/r_{ij})^6] + \sum_{i}^{N_p} (\mathrm{pH} - \mathrm{p}K_{a,i}) \ln 10 \tag{3}$$

where N and N_p run over all residues and protonated sites, respectively. κ^{-1} is the Debye length, λ_B = 0.7 nm (water, 298 K) is the Bjerrum length, z is particle valency (−1, 0, +1), $\beta\epsilon$ = 0.05 is the vdW strength,[15,29] σ_{ij} is the arithmetic mean particle diameter, r_{ij} is inter-residue distances, $\beta^{-1} = k_B T$ is the thermal

DOI: 10.1021/jp512027j
J. Phys. Chem. B 2015, 119, 503–508

energy, and $pK_{a,i}$ are the unperturbed acid dissociation constants for titratable amino acids. The magnitude of the short-ranged interaction, ϵ, has been chosen such that its effective contribution is the same as in a previously investigated model,[29] and we have made no attempts to fit it to the current case. The angularly averaged pair distribution function, $g(R) = \exp(-\beta w(R))$, is obtained by sampling the histogram of protein−protein mass center separations, R, and is subsequently integrated to give the osmotic second virial coefficient

$$B_2 = -2\pi \int_0^\infty (g(R) - 1)R^2 \, dR \tag{4}$$

The precision of the interaction free energy, $w(R)$, is $\pm 0.05\ k_BT$ or better for all relevant protein separations. To minimize noise amplification for large R when eq 4 is integrated, the tail of the sampled $g(R)$ is substituted with a smooth function at long separations where only Coulombic repulsion persists. The functional form is the linearized Poisson−Boltzmann result for two charged, macro-ions with charges smeared over their surfaces, $w(R)^{ion} = \lambda_B Z^2 \sinh^2(\kappa a) e^{-\kappa R}/R(\kappa a)^2$. Here Z is the average protein net charge and a an approximate protein radius, obtained by fitting to the $g(R)$ tail.

Finally, the inverse Debye length is calculated according to $\kappa = (8\pi\lambda_B I)^{1/2}$ where the ionic strength, $I = {}^1/_2 \sum_i \rho_i z_i^2$, is summed over all ion types of density ρ_i and valency z_i. Thus, for a 1:1 salt such as NaCl, I simply equals the salt concentration.

RESULTS AND DISCUSSION

This work was prompted by previous structure-based MC simulations on lactoferrin, which predicted the presence of an electrostatic anisotropic attraction.[15] The attraction came from a few localized amino acid residues that gave rise to an unusually distinct and narrow minimum in the interaction free energy as a function of protein−protein separation, $\beta w(R) = -\ln g(R)$. This is shown in Figure 2, and the minimum was found to deepen upon increasing pH toward the isoelectric point.[15] The involved amino acids identified in the simulations[15] are charged, pointing to a mechanism of electrostatic origin. Indeed, electrostatics was found to lock the two proteins into a few orientations, i.e., a regio-specific interaction. Using the angularly averaged protein−protein potential of mean force, we calculate B_2 as a function of pH, as shown in the inset to Figure 2. The minimum in $w(R)$ gives a negative contribution to B_2, which decreases with increasing pH. The simulations thus guide to the narrow set of conditions where to expect the interaction energy to display the minimum and electrostatic anisotropic attractions. They are expected at low ionic strength, near the isoelectric point which corresponds to B_2 values close to zero, as shown in the inset to Figure 2.

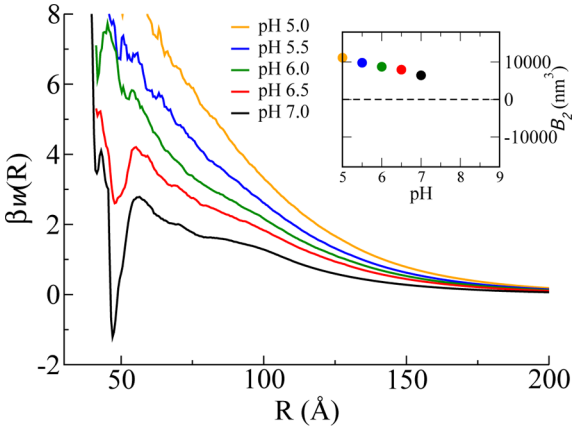

Figure 2. Simulated angularly averaged protein−protein potential of mean force, $\beta w(R)$, as a function of protein−protein mass center separation, R, and at different pHs. The salt concentration is 5 mM for all pHs. The inset shows the corresponding virial coefficients, B_2, cf. eq 4.

The experimental conditions corresponding to the simulations were investigated by performing static light scattering experiments as a function of protein concentration. Second virial coefficients were obtained from eq 1 (Methods) in a Debye representation of the scattered intensity, which is shown in Figure 3. Here K is an optical constant, C is the protein concentration and R_θ is the scattered light expressed as the excess Rayleigh ratio. The ionic strength is fixed at 5 mM while pH is varied. As shown in Figure 3 at pH 5.5, the charged proteins repel each other, resulting in a positive slope. This corresponds to a positive second virial coefficient, shown in the inset of Figure 3. By gradually increasing pH, while keeping the ionic strength fixed at 5 mM, we find the attractive and repulsive contributions to B_2 to balance out, at pH 7, resulting in a slightly negative B_2. Note that at pH 7 we switch to Tris buffer to maintain stable buffering capacity.

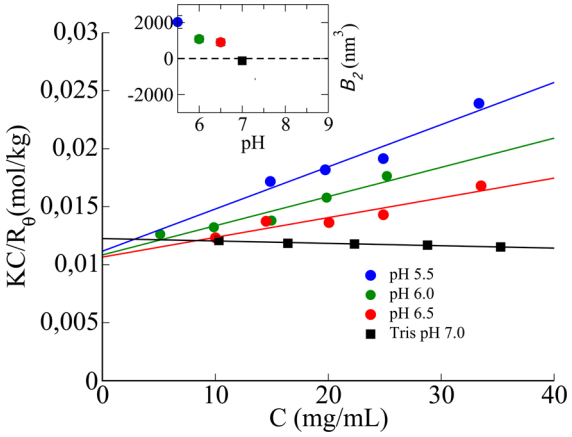

Figure 3. Debye plot at different pHs and constant ionic strength (5 mM) in acetate and Tris buffer (pH 7). The lines are weighted linear least-squares fits to the data. Error bars are included but lay within the symbols. The inset shows corresponding virial coefficients with error bars.

We next investigate how ionic strength influences the interactions, starting at 5 mM and pH 7. These are the ionic strength and pH conditions where the slope in Figure 3 turned negative, and where to expect the electrostatic patch attraction to be at its strongest, providing it is a real, measurable effect. The experimental results from static light scattering are shown in Figure 4. We observe how the slope, and correspondingly B_2, first decreases when the ionic strength is increased. This behavior is expected because electrostatic screening weakens the repulsion between proteins, resulting in a lowering of the slope and thus B_2. However, as more salt is added, surprisingly, the slope starts to *increase* at around 25 mM.

The corresponding second virial coefficients extracted from the experiments in Figure 4 are shown in the lower panel in Figure 5 as a function of ionic strength. The nonmonotonic dependence of the slope results in a B_2 minimum as a function of ionic strength.

DOI: 10.1021/jp512027j
J. Phys. Chem. B 2015, 119, 503−508

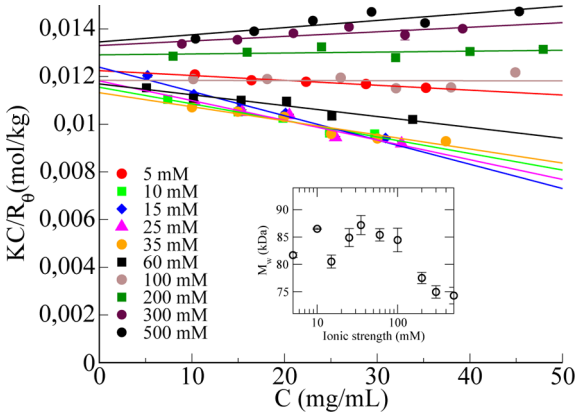

Figure 4. Debye plot at different ionic strengths at pH 7 in Tris buffer. The lines are weighted linear least-squares fits to the data. Error bars are included but lay within the symbols. The inset shows corresponding molecular weights as a function of ionic strength with error bars.

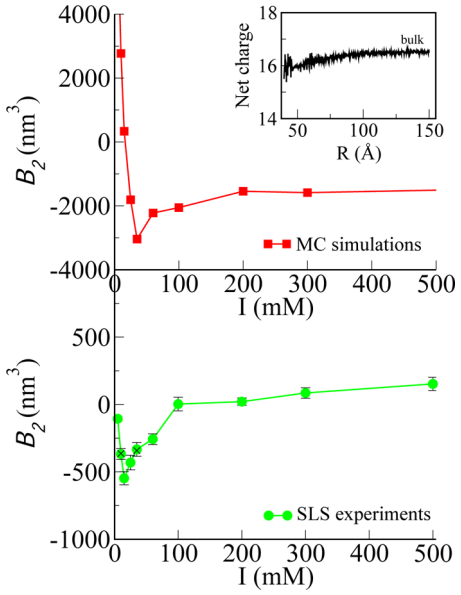

Figure 5. Calculated (top) and measured (bottom) second virial coefficient as a function of ionic strength, at pH 7. In the measurements, the ionic strengths 10 and 35 mM (shown as crosses) were repeated from additional concentration series and batches. The inset shows the calculated overall protein charge as a function of protein−protein mass center separation.

From the isolated experimental data, it would be difficult to determine which mechanism is responsible for the minimum. We also have B_2 values calculated from simulations at matching conditions; see the upper panel of Figure 5. Here, we observe exactly the same minimum in the B_2 values as a function of salt concentration. Importantly, we can directly link the minimum in B_2 to the minimum in the angularly averaged free energy, shown in Figure 2. The effect of salt on the angularly averaged potential of mean force is shown in Figure 6. It can be seen that addition of salt initially acts to expose the attractive minimum as the repulsive barrier at longer separations decreases. Additional salt screens both the repulsive barrier and the free energy minimum. The observed mechanism comes from two opposing, electrostatic contributions: a short-ranged, attractive patch and a long-ranged, screened Coulomb repulsion. Salt

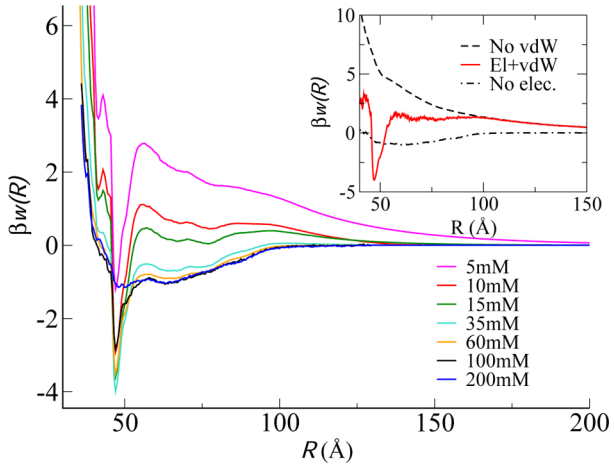

Figure 6. Angularly averaged protein−protein potential of mean force, $\beta w(R)$, at different salt concentrations, pH 7. The inset shows $\beta w(R)$ when either electrostatic or short-ranged, attractive ("vdW") interactions are artificially disabled at 5 mM and comparable conditions, pH 8.

initially screens the Coloumb repulsion, thus strengthening the effect of the attractive patch. As the salt concentration is further increased (decreasing Debye length), the attractive interaction is ultimately screened as well. This balance is manifested as a minimum in the second virial coefficient as a function of ionic strength, as observed in both SLS experiments and MC simulations.

Although the qualitative agreement between measured and simulated B_2 is excellent, the absolute values differ. This is expected from a coarse-grained model and we have deliberately made no attempts to fit the only free parameter in our model, the Lennard-Jones strength, ϵ, to the measurements. As also discussed in the Methodology, this single value is taken from a different protein system and essentially encompassed the net effect of all short-ranged, nonelectrostatic interactions. For this reason it is unlikely to be universal and as hinted at in a recent combined SAXS/simulation study of protein solution structure,[30] our choice of ϵ may be slightly too attractive but nonetheless close enough to capture complex, qualitative trends in arbitrary protein systems.

The inset to Figure 6 shows a study of the free energy, βw, as a function of the protein−protein separation. The βw, shown in red, where both electrostatic and short-ranged attractions are included, has a distinct and narrow minimum, corresponding to the tightly bound and stereospecific configuration.[15] Artificially turning off either electrostatic or short-ranged interactions suppresses the free energy minimum, showing that both interactions are needed due to nonlinear coupling of the Boltzmann weight.

An alternative explanation for the observed salt behavior of B_2 may stem from proton fluctuations. That is, a mechanism whereby the ionization states of the two proteins close to each other become correlated at low ionic strengths.[13,14] To assert if this mechanism is operating, we have analyzed the variation in protein charge as a function of separation. As shown in the inset of Figure 5, the net charge varies only weakly as the proteins approach. The slight decrease at shorter distance is a mutual response of the two approaching charge distributions. Hence, we conclude that fluctuation forces are unimportant for the present system as the average net charge of the proteins are only weakly perturbed.

DOI: 10.1021/jp512027j
J. Phys. Chem. B 2015, 119, 503−508

Other attractive protein interactions, signaled by a minimum in the second virial coefficient, have been reported[31,32] albeit at significantly higher salt concentrations. We argue that these observations cannot originate from the same electrostatic mechanism found here, because the ionic strength at which the attraction is located is too high to survive the electrostatic screening.

CONCLUSIONS

We have used static light scattering and computer simulations to obtain osmotic second virial coefficients, B_2, for lactoferrin as a function of pH and salt concentration. The simulations were used to guide the experiments to a narrow set of conditions where B_2 first decreases with added salt, then increases to reach a plateau. We show that this nonmonotonous behavior—observed unambiguously in experiment and simulations—originates from a high charge complementarity on the binding interface between two proteins. This creates a short-ranged attraction that is competing with a long-ranged repulsion due to the protein net charges. Addition of salt modulates the electrostatic screening length, whereby the balance between long- and short-ranged electrostatic interactions can be finely tuned. This study provides insight into how anisotropic protein attractions come about in a nonlinear combination of several electrostatic as well as other short-ranged forces.

AUTHOR INFORMATION

Corresponding Authors

*M. Lund. E-mail: mikael.lund@teokem.lu.se. Phone: +46 (0) 46 222 1428. Fax: +46 (0)46 222 8648.

*M. Zackrisson Oskolkova. E-mail: malin.zackrisson@fkem1.lu.se. Phone: +46 (0)46 222 8185. Fax: +46 (0)46 222 4413.

Notes

The authors declare no competing financial interest.

ACKNOWLEDGMENTS

The authors wish to thank the OMM Linneaus center in Lund; the Swedish Research Council; the Swedish Foundation for Strategic Research; the Crafoord Foundation; the Royal Swedish Academy of Sciences; LUNARC in Lund for computational resources; and Morinaga Milk Industry Co., Ltd, Japan for kindly providing us with the protein.

REFERENCES

(1) McManus, J.; Lomakin, A.; Ogun, O.; Pande, A.; Basan, M.; Pande, J.; Benedek, G. B. Altered Phase Diagram Due to a Single Point Mutation in Human γD-Crystallin. *Proc. Natl. Acad. Sci. U. S. A.* **2007**, *104*, 16856−16861.

(2) Mezzenga, R.; Fischer, P. The Self-Assembly, Aggregation and Phase Transition of Food Protein Systems in One, Two and Three Dimensions. *Rep. Prog. Phys.* **2013**, *76*, 046601.

(3) Piazza, R. Protein Interactions and Association: an Open Challenge for Colloid Science. *Curr. Opin. Colloid Interface Sci.* **2004**, *8*, 515−522.

(4) Piazza, R. Interactions and Phase Transitions in Protein Solutions. *Curr. Opin. Colloid Interface Sci.* **2000**, *5*, 38−43.

(5) Fusco, D.; Headd, J. J.; de Simone, A.; Wang, J.; Charbonneau, P. Characterizing Protein Crystal Contacts and Their Role in Crystallization: Rubredoxin as a Case Study. *Soft Matter* **2014**, *10*, 290−302.

(6) Dumetz, A. C.; Snellinger-O'Brien, A. M.; Kaler, E. W.; Lenhoff, A. M. Patterns of Protein-Protein Interactions in Salt Solutions and Implications for Protein Crystallization. *Protein Sci.* **2007**, *16*, 1867−1877.

(7) Price, W. N.; Chen, Y.; Handelman, S. K.; Neely, H.; Manor, P.; Karlin, R.; Nair, R.; Liu, J.; Baran, M.; Everett, J.; et al. Understanding the Physical Properties that Control Protein Crystallization by Analysis of Large-Scale Experimental Data. *Nat. Biotechnol.* **2009**, *27*, 51−57.

(8) Wertheim, M. S. Fluids with Highly Directional Forces. I. Statistical Thermodynamics. *J. Stat. Phys.* **1984**, *35*, 19−34.

(9) Kern, N.; Frenkel, D. Fluid-Fluid Coexistence in Colloidal Systems with Short-Ranged Strongly Directional Attraction. *J. Chem. Phys.* **2003**, *118*, 9882−9889.

(10) Bianchi, E.; Largo, J.; Tartaglia, P.; Zaccarelli, E.; Sciortino, F. Phase Diagram of Patchy Colloids: Towards Empty Liquids. *Phys. Rev. Lett.* **2006**, *97*, 168301.

(11) Bianchi, E.; Tartaglia, P.; Zaccarelli, E.; Sciortino, F. Theoretical and Numerical Study of the Phase Diagram of Patchy Colloids: Ordered and Disordered Patch Arrangements. *J. Chem. Phys.* **2008**, *128*, 144504.

(12) Munao, G.; Preisler, Z.; Vissers, T.; Smallenberg, F.; Sciortino, F. Cluster Formation in One-Patch Colloids: Low Coverage Results. *Soft Matter* **2013**, *9*, 2652−2661.

(13) Kirkwood, J. G.; Shumaker, J. B. Forces Between Protein Molecules in Solution Arising from Fluctuations in Proton Charge and Configuration. *Proc. Natl. Acad. Sci. U. S. A.* **1952**, *38*, 863−871.

(14) Lund, M.; Jönsson, B. Charge Regulation in Biomolecular Solution. *Q. Rev. Biophys.* **2013**, *46*, 265−281.

(15) Persson, B. A.; Lund, M.; Forsman, J.; Chatterton, D. E. W.; Åkesson, T. Molecular Evidence of Stereo-Specific Lactoferrin Dimers in Solution. *J. Biophys. Chem.* **2010**, *151*, 187−189.

(16) Neal, B. L.; Asthagiri, D.; Velev, O. D.; Lenhoff, A. M.; Kaler, E. W. Why Is the Osmotic Second Virial Coefficient Related to Protein Crystallization? *J. Cryst. Growth* **1999**, *196*, 377−387.

(17) Dumetz, A. C.; Chockla, A. M.; Kaler, E. W.; Lenhoff, A. M. Effects of pH on Protein-Protein Interactions and Implications for Protein Phase Behavior. *Biochim. Biophys. Acta* **2008**, *1784*, 600−610.

(18) Roberts, R.; Keeling, R.; Tracka, M.; van der Walle, C. F.; Uddin, S.; Warwicker, J.; Curtis, R. The Role of Electrostatics in Protein-Protein Interactions of a Monoclonal Antibody. *Mol. Pharmaceutics* **2014**, *11*, 2475−2489.

(19) Baker, E. N.; Baker, H. M. A structural Framework for Understanding the Multifunctional Character of Lactoferrin. *Biochimie* **2009**, *91*, 3−10.

(20) Brock, J. H. The Physiology of Lactoferrin. *Biochem. Cell Biol.* **2002**, *80*, 1−6.

(21) Lönnerdal, B.; Iyer, S. Lactoferrin Molecular Structure and Biological Function. *Annu. Rev. Nutr.* **1995**, *15*, 93−110.

(22) Babina, S. E.; Tuzikov, F. V.; Tuzikova, N. A.; Buneva, V. N.; Nevinskii, G. A. Effect of Nucleotides on the Oligomeric State of Human Lactoferrin. *Mol. Biol. (Moscow, Russ. Fed., Engl. Ed.)* **2006**, *40*, 121−131.

(23) Superti, F.; Siciliano, R.; Rega, B.; Giansanti, F.; Valenti, P.; Antonini, G. Involvement of Bovine Lactoferrin Metal Saturation, Silica Acid and Protein Fragments in the Inhibition of Rotavirus Infection. *Biochim. Biophys. Acta* **2001**, *1528*, 107−115.

(24) Roosen-Runge, F.; Heck, B. S.; Zhang, F.; Kohlbacher, O.; Schreiber, F. Interplay of pH and Binding of Multivalent Metal Ions: Charge Inversion and Reentrant Condensation in Protein Solutions. *J. Phys. Chem. B* **2013**, *117*, 5777−5787.

(25) Provencher, S. W. A. Constrained Regularization Method for Inverting Data Represented by Linear Algebraic or Integral Equations. *Comput. Phys. Commun.* **1982**, *27*, 213−227.

(26) Provencher, S. W. CONTIN: A General Purpose Constrained Regularization Program for Inverting Noisy Linear Algebraic and Integral Equations. *Comput. Phys. Commun.* **1982**, *27*, 229−242.

(27) Zhao, H.; Brown, P. H.; Schuck, P. On the Distribution of Protein Refractive Index Increments. *Biophys. J.* **2011**, *100*, 2309−2317.

(28) Metropolis, N. A.; Rosenbluth, A. W.; Teller, M. N. R. A.; Teller, E. Equation of State Calculations by Fast Computing Machines. *J. Chem. Phys.* **1953**, *21*, 1087−1092.

DOI: 10.1021/jp512027j
J. Phys. Chem. B 2015, 119, 503−508

(29) Lund, M.; Jönsson, B. A Mesoscopic Model for Protein-Protein Interactions in Solution. *Biophys. J.* **2003**, *85*, 2940−2947.
(30) Kaieda, S.; Lund, M.; Plivelic, T. S.; Halle, B. Weak Self-Interactions of Globular Proteins Studied by Small-Angle X-ray Scattering and Structure-Based Modeling. *J. Phys. Chem. B* **2014**, *118*, 10111−10119.
(31) Petsev, D. N.; Vekilov, P. G. Evidence for Non-DLVO Hydration Interactions in Solutions of the Protein Apoferritin. *Phys. Rev. Lett.* **2000**, *84*, 1339.
(32) Piazza, R.; Iacopini, S.; Galliano, M. BLGA Protein Solutions at High Ionic Strength: Vanishing Attractive Interactions and "Frustrated" Aggregation. *Europhys. Lett.* **2002**, *59*, 149−154.

DOI: 10.1021/jp512027j
J. Phys. Chem. B 2015, 119, 503−508